ANALYSIS OF CLASS OF NONLINEAR SYSTEM UNDER DETERMINISTIC AND STOCHASTIC EXCITATIONS

By Michael A. Tognarelli[1] and Ahsan Kareem[2]

ABSTRACT: In this paper, some analysis techniques of nonlinear dynamics are applied to physical systems which may be modeled by the Duffing nonlinear differential equation. The response of the Duffing oscillator to both deterministic sinusoidal and stochastic loadings is investigated and distinct regimes of the response motion are discerned and discussed. The stochastic input to the system is low-pass Gaussian white noise. The efficacy of studying the variation in time of the probability density of one or more of the system output states to determine the type of motion of the system is examined. Attractors in phase space are defined via Poincaré mapping and bounds on motion which serve as signatures for particular types of motion (e.g., chaotic, periodic) are identified by a hypervolume measurement technique. An accepted method for adapting one measured output state into a higher dimensional space by using time-delayed coordinates is used in conjunction with correlation dimension calculation to supply a lower-bound estimate of the fractal dimension and insight into the character of the motion of a nonlinear dynamic system.

INTRODUCTION

Many mechanical systems involving fluid-structure interaction may be modeled by the nonautonomous Duffing oscillator

$$\ddot{y} + b\dot{y} + cy + dy^3 = f(t) \tag{1}$$

For example, the rolling motion of ships (e.g., Ding et al. 1994) or the motion of bluff bodies in an aerodynamic flow (e.g., Sekar and Narayanan 1994). In addition, nonlinear dynamical equations, such as the Mathieu equation have been used to model the heave (vertical) motion of a floating offshore platform (Jeffreys 1988). It has been observed by several authors (e.g., Kapitaniak 1988) that the response of (1) to both purely deterministic loading and deterministic loading superimposed by Gaussian white noise may be periodic or chaotic in nature. In this study, it is desired to propose a framework within which to investigate models for practical problems such as those just mentioned. Through such a framework, it may also be possible to enhance modeled systems by identifying deterministic mechanisms underlying experimental data which may appear random, at first glance.

The autonomous system of (1) can be cast in the following form:

$$\frac{dx}{dt} = y \tag{2a}$$

$$\frac{dy}{dt} = -by - cx - dx^3 \tag{2b}$$

which has the sole equilibrium point (0, 0) when c and d have the same sign, but has two additional equilibrium points, $(\pm\sqrt{-(c/d)}, 0)$, when the two parameters have opposite signs. The Jacobian matrix of the first derivatives of this system is

$$A = \begin{bmatrix} 0 & 1 \\ c - 3dx^2 & -b \end{bmatrix} \tag{3}$$

Linear stability analysis indicates that the eigenvalues of (3) for $x = 0$ are

$$\lambda_{1,2} = \frac{1}{2}(-b \pm \sqrt{b - 4dr_{cd}}) \tag{4}$$

where $r_{cd} = c/d$. When $x = \sqrt{-r_{cd}}$, the eigenvalues of (3) are

$$\lambda_{1,2} = \frac{1}{2}(-b \pm \sqrt{b + 8dr_{cd}}) \tag{5}$$

Clearly, the linear stability of the equilibrium points, assuming that the damping coefficient, b, is positive, depends directly upon the signs and ratio of the coefficients of the linear and cubic stiffness terms as shown in Fig. 1. Fig. 2 illustrates state

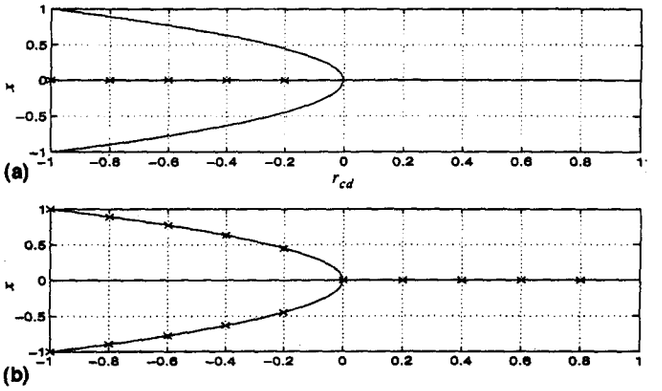

FIG. 1. Bifurcation Diagrams in Plane $y = 0$ for Linear Stability Analysis of Autonomous Duffing Oscillator, Eq. (2): (a) Illustrates Case for $d > 0$; (b) Illustrates Case for $d < 0$ (Hatched Areas Are Unstable)

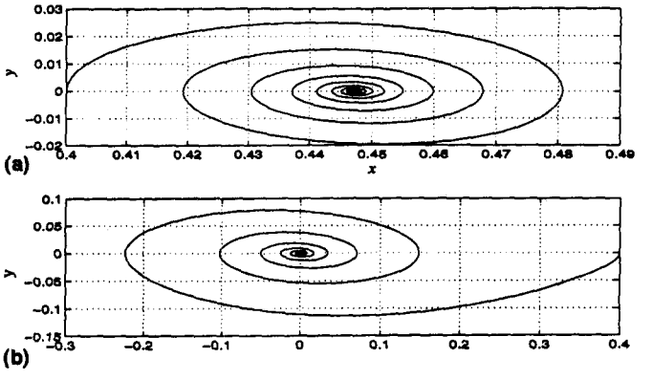

FIG. 2. State Space Trajectories of System, Eq. (2): (a) $d > 0$, $c < 0$; (b) $d < 0$, $c > 0$

[1]Doctoral Candidate, Dept. Civ. Engrg. and Geo. Sci., Univ. of Notre Dame, 156 Fitzpatrick Hall, Notre Dame, IN 46556-0767.

[2]Prof., Dept. Civ. Engrg. and Geo. Sci., Univ. of Notre Dame, 156 Fitzpatrick Hall, Notre Dame, IN.

Note. Discussion open until March 1, 1998. To extend the closing date one month, a written request must be filed with the ASCE Manager of Journals. The manuscript for this paper was submitted for review and possible publication on June 2, 1997. This paper is part of the ***Journal of Aerospace Engineering***, Vol. 10, No. 4, October, 1997. ©ASCE, ISSN 0893-1321/97/0004-0162-0172/$4.00 + $.50 per page. Paper No. 15919.

trajectories of the system (2) with initial conditions $x = 0.4$, $y = 0$, and parameters, $b = 0.1$, $c = \mp 0.2$, $d = \pm 1.0$. The dependence on the coefficients of the stiffness terms that is predicted in Fig. 1 is evident in the convergence of the solution to two distinct stable points in Fig. 2.

In many practical situations, however, the systems which we model with the Duffing oscillator are driven by outside excitation which may be both deterministic and stochastic in nature. For example, an offshore platform is excited by hydrodynamic wave forces while a cylindrical power cable oscillates under the influence of aerodynamic wind forces, both of which have deterministic and random components. We must depart from the preceding linear stability analysis for autonomous systems and examine these types of nonautonomous systems in the context of the techniques outlined in the forthcoming sections. The application of these analysis methods requires the time-domain simulation of the Duffing system as well as deterministic and stochastic processes.

Simulations of the systems described in this paper were accomplished using the SIMULINK Toolbox (*SIMULINK* 1992) in conjunction with MATLAB 4.2c (*MATLAB* 1992). Within the SIMULINK framework, the dynamic system was cast in the form of a block diagram which receives input from an independent code, integrates the system using a fifth-order Runge-Kutta scheme with a maximum time-step of $\pi/20$ (1/40 times the natural period of the deterministic input), and outputs the response states. The deterministic harmonic inputs to this system were developed by straightforward applications of intrinsic functions of the software. The additive Gaussian white noise used as the random input in the following discussion is actually low-pass white noise having a constant power spectral density over $0 < \omega \leq \omega_c$. Thus, it has a finite variance and a cutoff frequency of $\omega_c = \pi/\Delta t$, where Δt is the simulation time step.

DISCUSSION

Probability Density Function as Function of Time

The probability density function (PDF) of the response of a nonlinear system perturbed by random noise can exhibit multimaxima (Kapitaniak 1988). The appearance of multiple maxima can correspond to a bifurcation in the solution of the deterministic system. This phenomenon can also arise when no bifurcation is present in the linear stability analysis of the deterministic system. As such, although chaotic behavior of a system influenced by stochastic noise is characterized by a response PDF possessing multimaxima, this characteristic alone is not sufficient to indicate the onset of chaos. This is shown in Fig. 3 for the case of a deterministic Duffing oscillator where multimaxima behavior is clear in the system PDF,

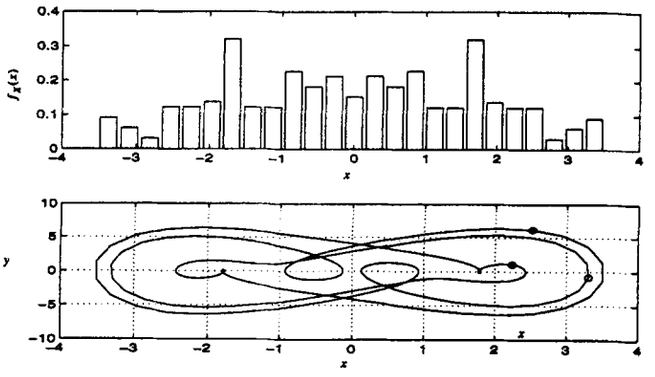

FIG. 3. Multimaxima PDF and Trajectories for Duffing Oscillator with Periodic Response (Circular Symbols Indicate Poincaré Mapping)

but the system trajectories indicate that the motion is, in fact, periodic.

The distinction between the PDF of a chaotic response of a perturbed Duffing system and a regular periodic response may be made by noting that for chaos, the probability density not only exhibits multimaxima, but also experiences change over time. Thus, a plot of the probability density of a given state value at one time, $f_x(x, t)$, versus its value at some time later, $f_x(x, t + \tau)$, for a given realization would provide the additional insight necessary to delineate chaotic response from regular response. That is, if the value of the probability density for a given state remains constant over the range of time, the motion

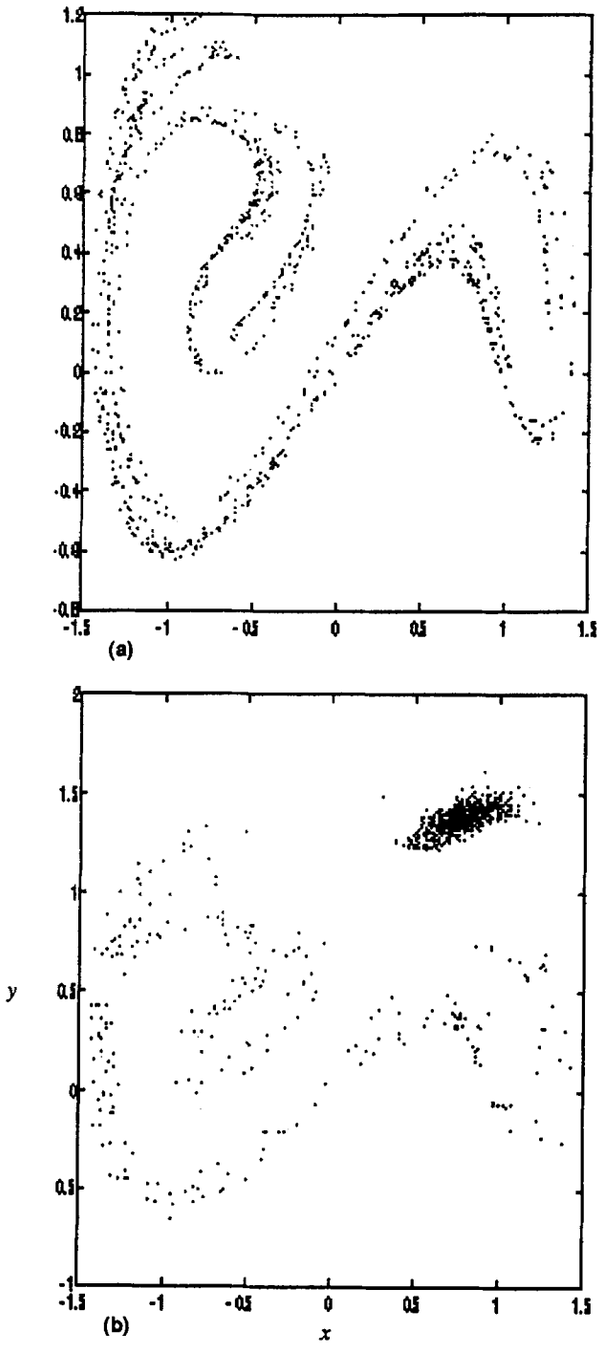

FIG. 4. (a) Realization of Poincaré Map for Duffing System Described in Text with Additional Gaussian White Noise of Standard Deviation 0.01; (b) Realization of Poincaré Map for Same System when Standard Deviation of White Noise Is 0.1

is periodic. Otherwise, it is chaotic. For the oscillator (1) excited by

$$f(t) = 0.3 \cos t + W(t) \tag{6}$$

where $W(t)$ = low-pass Gaussian white noise with standard deviation of 0.0032 (for comparison's sake the standard deviation of the sinusoidal excitation is 0.387), it is possible to discern chaotic from periodic motions in this way. However, the level of noise allowable before the two types of system behavior become indistinguishable is too small for practical applications in which random excitation plays a more significant role. A further difficulty arises when the trajectories of a given system are drawn into multiple basins of attraction during the course of a realization of the response due to the perturbation introducted by additive noise. For such cases, even though the neighboring attractors may be periodic, changes in the PDF can be significant, and in the context of the present discussion, misleading.

Averaged Poincaré Map

For a nonautonomous system driven by harmonic input, the Poincaré mapping is defined as the transformation (e.g., Thompson and Stewart 1986)

$$x_{i+1} = F(x_i) \tag{7}$$

where x_{i+1} = states of the system exactly one time period of the excitation after the states, x_i, have occurred. A more rigorous mathematical definition of this mapping may be found in Kapitaniak (1988). By iterated application of this mapping to a nonlinear system with given initial conditions, we can graphically characterize the regularity of motion of the system and describe its attractors.

When a harmonically driven system is perturbed by the additional excitation of a random noise, however, the Poincaré mapping for each realization is different. In these cases, it is possible to define an average or mean Poincare map (Kapitaniak 1988). This is essentially done by averaging the state values at corresponding multiples of the natural period of the deterministic component of the excitation for several realizations of the system response. Ultimately, then, the mean Poincaré map is

$$E[x_{i+1}] = F(E[x_i]) \tag{8}$$

where $E[x_i]$ = the expected value of the states at the ith integral multiple of the natural period of the harmonic excitation taken over all realizations. Examples of realizations of the Poincaré map for the Duffing system (1) with $b = 0.14$, $c = -1.0$, $d = 1.0$, and the same excitation described in the preceding section are shown in Fig. 4 for cases when the standard deviation of the Gaussian white noise has values of 0.01 and 0.1. Although these realizations indicate that some orderly structure is preserved for significant values of additive random excitation, the maps computed by averaging the realization as indicated in (8), bear no resemblance to the expected results from the deterministic system [shown in Fig. 7(a)]. This may be the result of the phenomenon noted in Fig. 4(b), where for this realization two distinct attractors may be observed to govern the system motion. The appearance of this type of behavior, wherein different attractors may appear separately or in tandem for a given realization of the response process, could feasibly act to complicate any attempt to arrive at a meaningful overall averaged result.

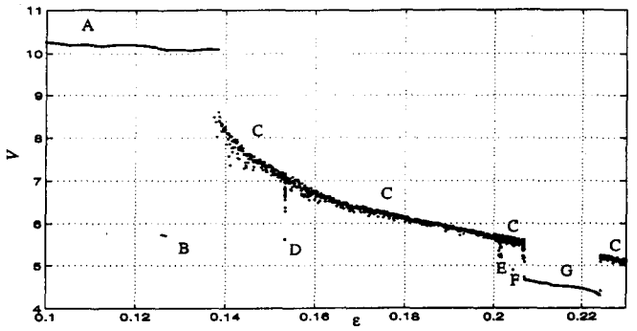

FIG. 5. Hypervolume Plot for Deterministic System, Eq. (9) with Regimes of Periodic and Chaotic Motion Indicated by A, B, C, D, E, F, G

Hypervolume Method

A further means of characterizing the behavior of a nonlinear system involves consideration of the bounds of its motion in phase space. Vaneck (1994) has illustrated a hypervolume calculation technique for deterministically excited systems whereby the bounds of a simulated posttransient response mo-

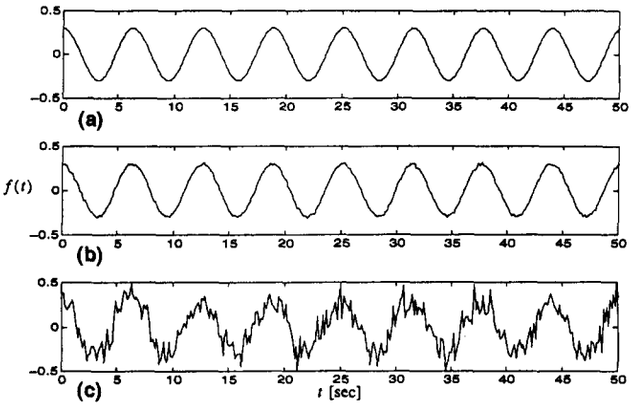

FIG. 6. Sample Input Time Histories: (a) Deterministic Cosine; (b) Deterministic Cosine Plus Low-Pass White Noise, $\sigma_{ww} = 0.01$; (c) Deterministic Cosine Plus Low-Pass White Noise, $\sigma_{ww} = 0.1$

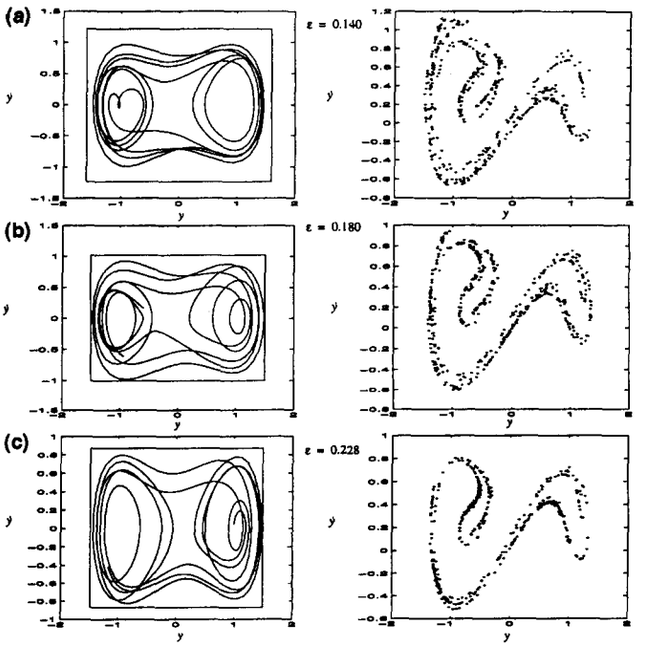

FIG. 7. Trajectories and Strange Attractors for Three Chaos Regimes of Eq. (9); Hypervolumes Are as Indicated (Deterministic Case)

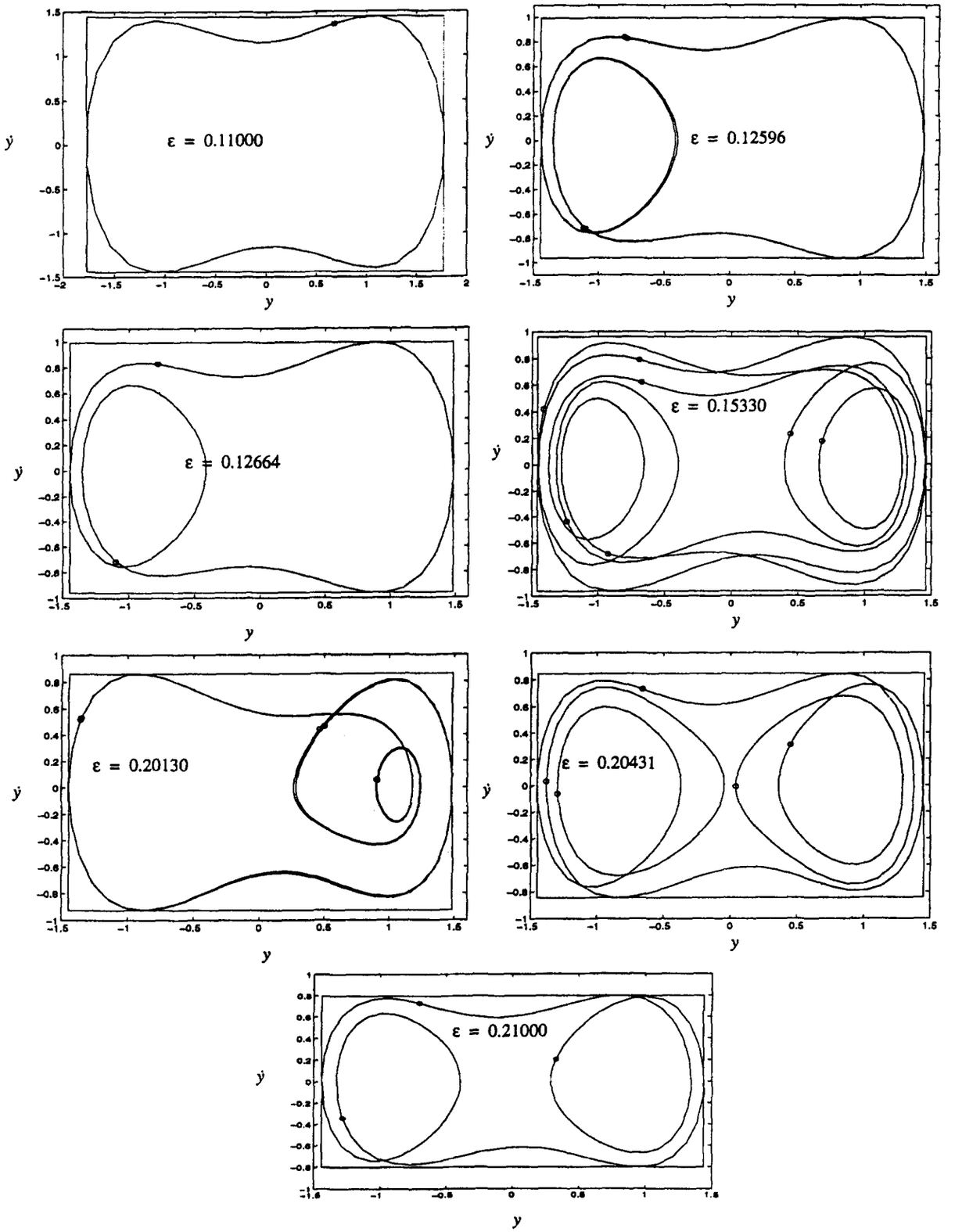

FIG. 8. Trajectories and Poincaré Maps for Periodic Motion of Eq. (9) in Regimes A, B ($n = 2$), B ($n = 4$), D, E, F, G; Enclosing Hypervolume Is Indicated as Well (Deterministic Case)

tion are quantified and employed to define the hypervolume in phase space which entirely contains the system motion. The term 'hypervolume' implies that the analysis may be extended to any finite-dimensional space. Indeed, in two-dimensional phase space we are dealing with a bounding area. By noting jumps in the value of the hypervolume over a range of parameters, we may detect transitions of the motion between periodic and chaotic behavior (see Fig. 5).

Starting with the Duffing oscillator example of Vaneck (1994)

$$\ddot{y} + \varepsilon\dot{y} + y(y^2 - 1) = \gamma \cos \omega t \tag{9}$$

which has already been employed to demonstrate some of the techniques previously discussed, we seek to extend this study to systems with additive noise in the forcing term. Examples of the input to the system are shown in Fig. 6. For $\gamma = 0.3$, $\omega = 1$, and initial conditions $(y_0, \dot{y}_0) = (0.1, 0.0)$, the system analysis in the deterministic case is first replicated in Fig. 5 for a range of $0.10 \leq \varepsilon < 0.23$. For this case, the hypervolume in question is equal to

$$V = (y_{max} - y_{min})(\dot{y}_{max} - \dot{y}_{min}) \tag{10}$$

and several regimes of motion are clear in the figure. Regime A is characterized by periodic motion. Regime B contains areas of periodic motion of subharmonic orders four and two. (For a periodic response, subharmonic order is the number of natural periods of the excitation which are required to complete a full cycle of the response.) Regimes C are chaotic, and regime D is periodic motion of subharmonic order seven. Regime E is periodic motion of subharmonic order six. Regime F is periodic motion of subharmonic order five, and regime G is periodic motion of subharmonic order five. In this study, regime B was identified by refining the discretization of ε to values as small as $\Delta\varepsilon = 1 \times 10^{-5}$, where no jump had been seen in previous investigations, bringing to light the importance of clearly defining the modeled system, as well as the extent to which this method may become painstaking if all regimes are to be included in a particular analysis. Additionally, for regime B, although two distinct types of periodic motion were detected, no jump in hypervolume signaled the transition within the regime. Examples of the trajectories, Poincaré maps, and hypervolumes for the chaotic regimes are given in Fig. 7. Examples for the periodic regimes of motion (A, B, D, E, F, G) are given in Fig. 8.

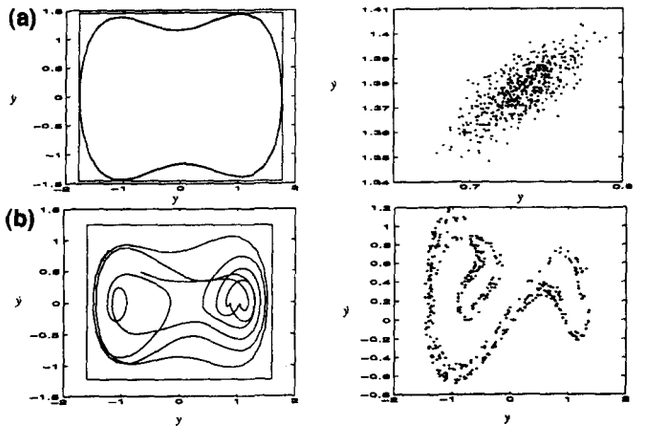

FIG. 9. Trajectories and Poincaré Mapping Typical of Behavior of Eq. (9) for an Additional Gaussian White Noise having Standard Deviation 0.01: (a) in Regime A; (b) in Regime C

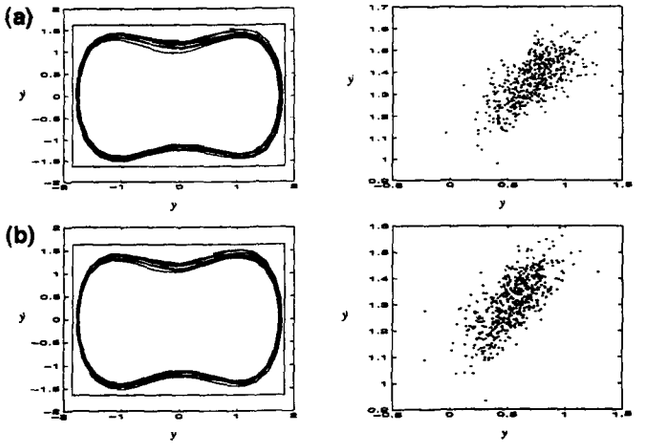

FIG. 10. Trajectories and Poincare Mappings Typical of Behavior of Eq. (9) for an Additional Gaussian White Noise Having Standard Deviation 0.1: (a) in Regime A; (b) in Regime C

It is desired, then, to determine whether this method can be as effective in identifying different regimes of motion for cases when the deterministic excitation is coupled with a stochastic process. Observing Fig. 9, it is seen that for the adjacent periodic and chaotic motions represented by 0.125 (regime A) and 0.140 (regime C), the two types of motion are still distinguishable from one another for an added stochastic excitation having standard deviation 0.01. The hypervolumes for these cases are 10.3 for the periodic motion and 7.9 for the chaotic motion. However, when the noise standard deviation is increased to 0.1 as shown in Fig. 10, the two responses seem to exhibit similar behavior, a description of which might be

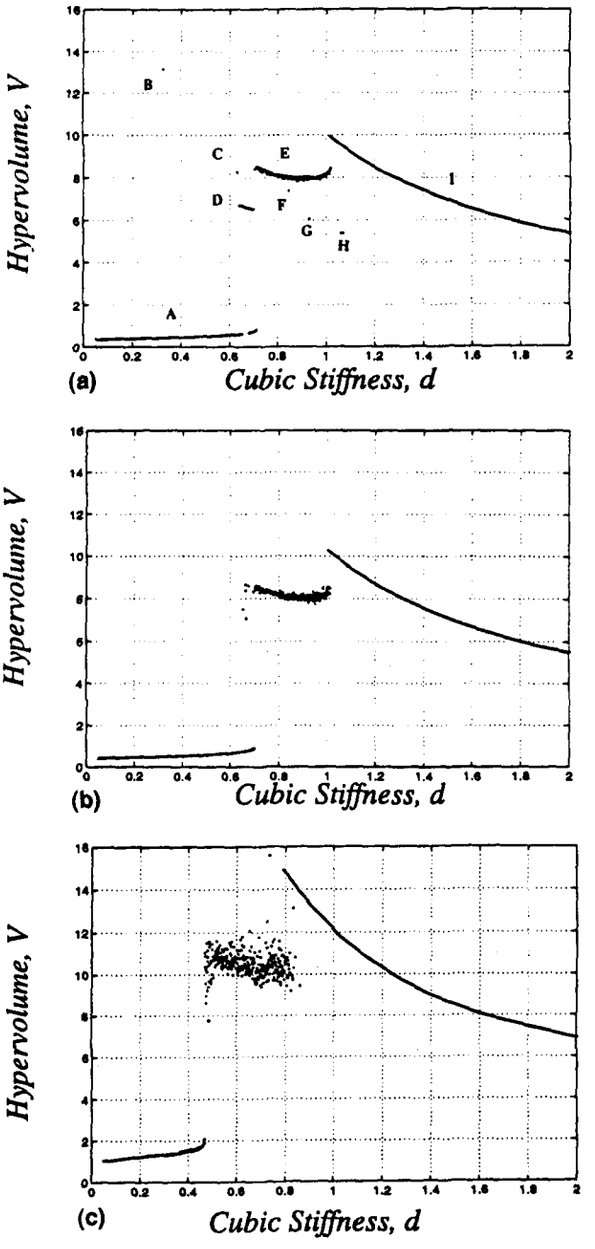

FIG. 11. Hypervolume as It Varies with Cubic Stiffness for System Described by Eq. (1): (a) Deterministic Excitation; (b) Deterministic Plus White Noise Excitation ($\sigma_{ww} = 0.01$); (c) Deterministic Plus White Noise Excitation ($\sigma_{ww} = 0.1$)

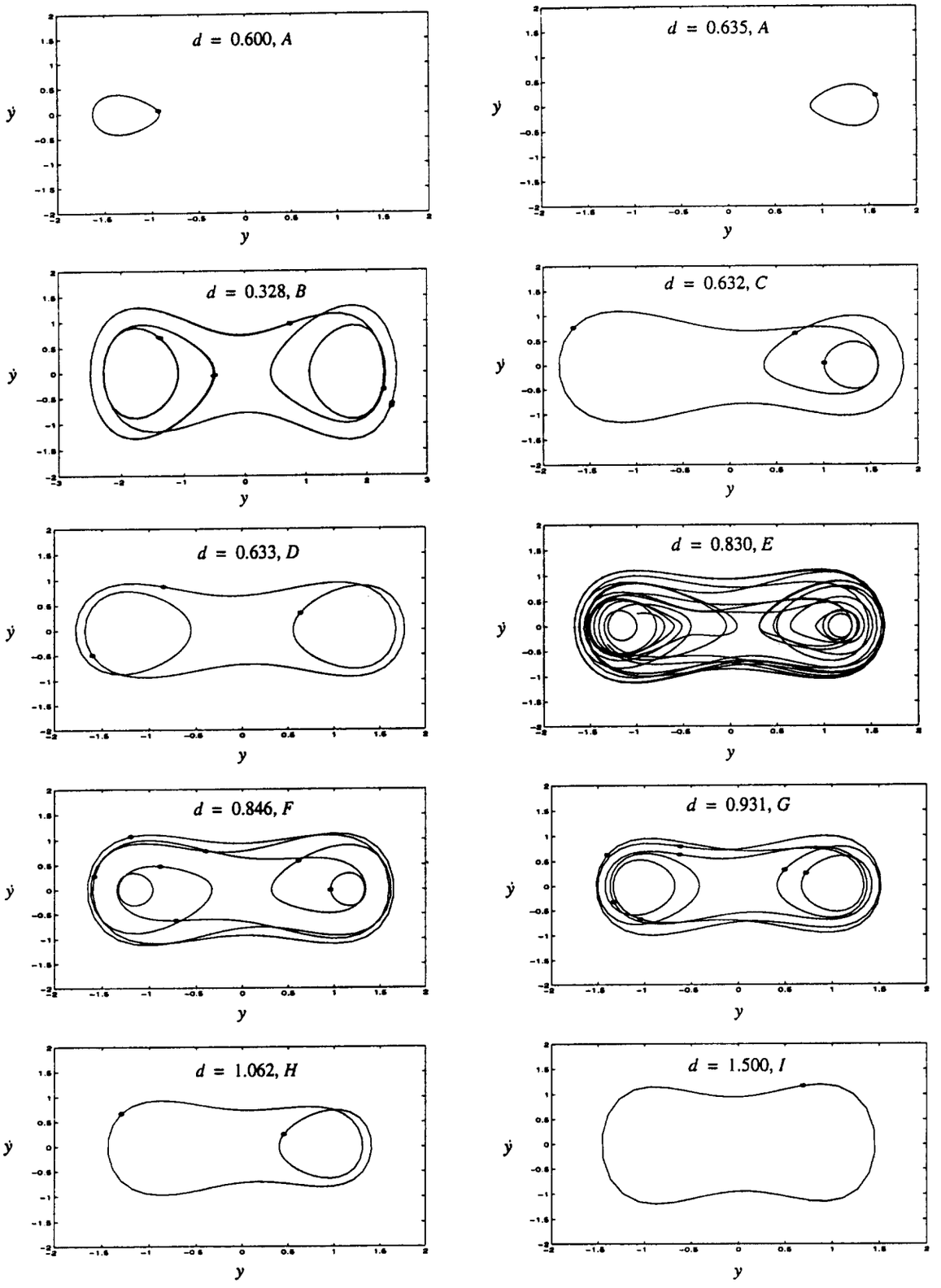

FIG. 12. Trajectories/Poincaré Maps for Eq. (1) over Range of Duffing Stiffness, d (Deterministic Case)

'smeared periodic' motion. Both responses possess bounding hypervolumes of 12.1 and Poincaré maps which nearly coalesce to a single point (note axis scaling on attractor portraits).

To examine both the utility, as well as the limitations of the hypervolume technique for systems excited by both deterministic and random processes, consider again (1), where $a = 1.00$, $c = -1.00$, the damping is fixed as $b = 0.14$, the initial conditions are (0.1, 0.0), the input to the system, $f(t)$, is given in (6), and the Duffing stiffness parameter is varied over the range, $0.05 \leq d \leq 2.00$. Fig. 11 illustrates how the hypervolume varies with the Duffing stiffness parameter for three different excitation scenarios. For the case of purely deterministic excitation, nine distinct regimes of motion can be detected using the hypervolume technique. When a low intensity, low-

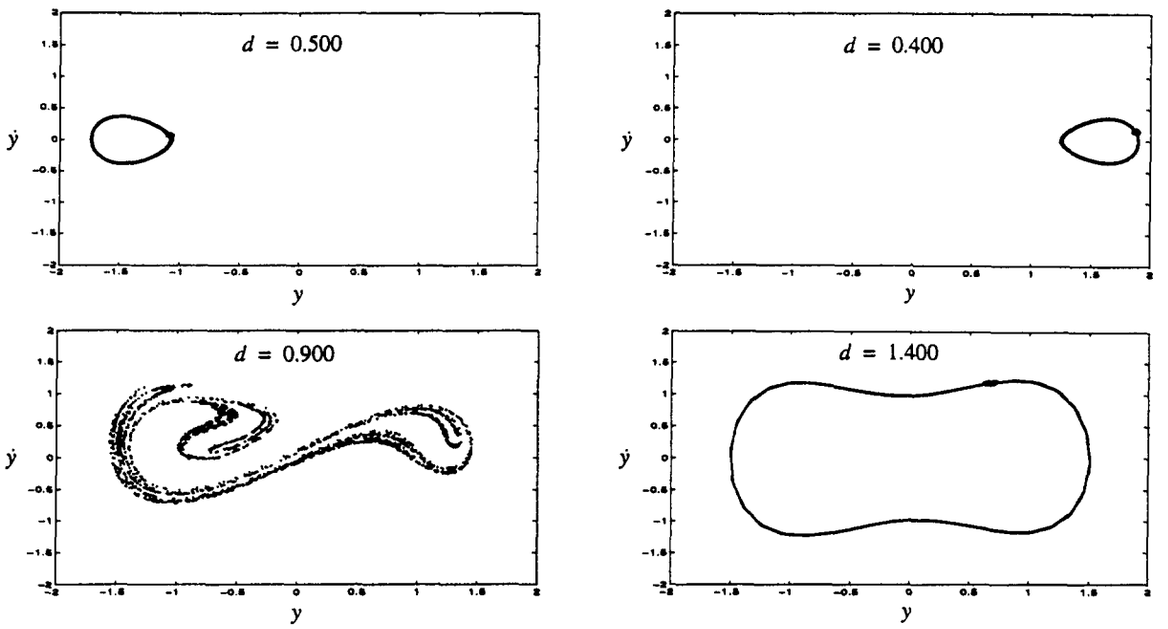

FIG. 13. Trajectories/Poincaré Maps for Eq. (1) over Range of Duffing Stiffness, d; For Chaotic Regime, Only Poincaré Map Is Shown ($\sigma_{ww} = 0.01$)

pass white noise is added to the excitation, many of these regimes are no longer observed. As the intensity level of the white noise is increased, three distinct regimes are still noticeable, but the data appears significantly more scattered than for the previous cases. While the hypervolume technique succeeds in signaling overall changes in the character of the largest attractor in the system response, for the cases in which the response is continuously perturbed by the presence of white noise input, it cannot indicate when the trajectories are influenced by different attractors. This issue will be addressed in a forthcoming discussion.

Fig. 12 illustrates trajectories and Poincaré maps for the various regimes detected in the case when the input to the system is purely a deterministic cosine wave. Presently, referring to Fig. 11 for the alphabetical regime labels, A–I, two types of periodic motion having the same period as the excitation are noted in regime A. Regime B represents periodic motion of subharmonic order ten. Regimes C and D both represent motion of subharmonic order three, but the trajectories of the motion found in regime D are significantly more compact than those of regime C. Regime E is chaotic motion and surrounds regimes F and G, both of which represent periodic motion of order seven. Finally, regime H represents periodic motion of subharmonic order two and regime I represents periodic motion of subharmonic order one.

Fig. 13 shows phase space trajectories and Poincaré maps for the case in which the sinusoidal input is superimposed by a low-pass white noise having standard deviation, $\sigma_{ww} = 0.01$. The periodic regimes of motion are similar to some of those appearing in Fig. 12 with the exception that the noise perturbs the system motion such that it does not repeat itself exactly by following a single closed curve in phase space. Rather, for such cases, the smeared periodic motion occupies bands of phase space and some scatter is noticeable in the Poincaré mappings. This is less noticeable in the chaotic regime of motion. A problem with the hypervolume technique is noted in Fig. 14 in which a time history of the motion of the system described by (1) for $d = 0.702$ is shown. Clearly visible are three distinct regimes of motion, two periodic and one chaotic, each lasting up to several minutes. Hypervolume analysis of this realization captures only that regime of motion which occupies the largest area of phase space, here, the chaotic motion. Without making a closer examination of the time history of the motion, it is impossible to tell via the hypervolume technique that multiple regimes of motion are coexisting. This phenomenon occurs for many values of the Duffing stiffness parameter, d.

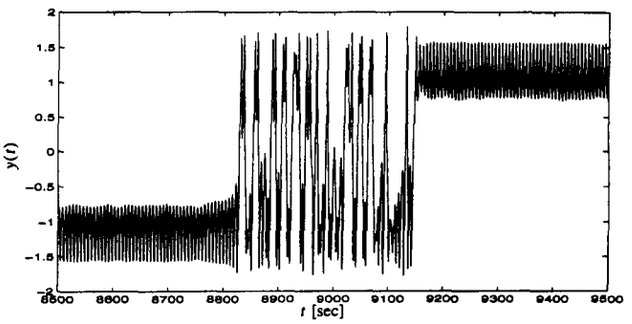

FIG. 14. Time History, $\sigma_{ww} = 0.01$, $d = 0.702$, which Indicate Presence of Multiple Regimes of Motion for Response to Eq. (1)

Fig. 15 contains trajectories and Poincaré maps from three separate motion regimes of (1) when the white noise level is increased to $\sigma_{ww} = 0.10$. Here, separate motion types are still detectable, but the problem discussed in the previous paragraph becomes more widespread as the level to which the system is perturbed is increased. This is evident in the case of the attractor shown in the upper right portion of the figure where two darker, more heavily populated areas indicate the scattered Poincaré maps of two smeared periodic regimes of motion which occur along with the chaotic regimes which is characterized by the larger strange attractor.

Time-Delay Adaptation of Scalar Signal to Multidimensional Space

Often in characterizing the motion of nonlinear dynamic systems, it is desirable to note the dimension of the space occupied by a response process. As described in a forthcoming section, however, in order to characterize the dimension of a particular attractor, a state space must be worked with which is of equal or greater dimension than that occupied by the attractor. When the required number of states is not available

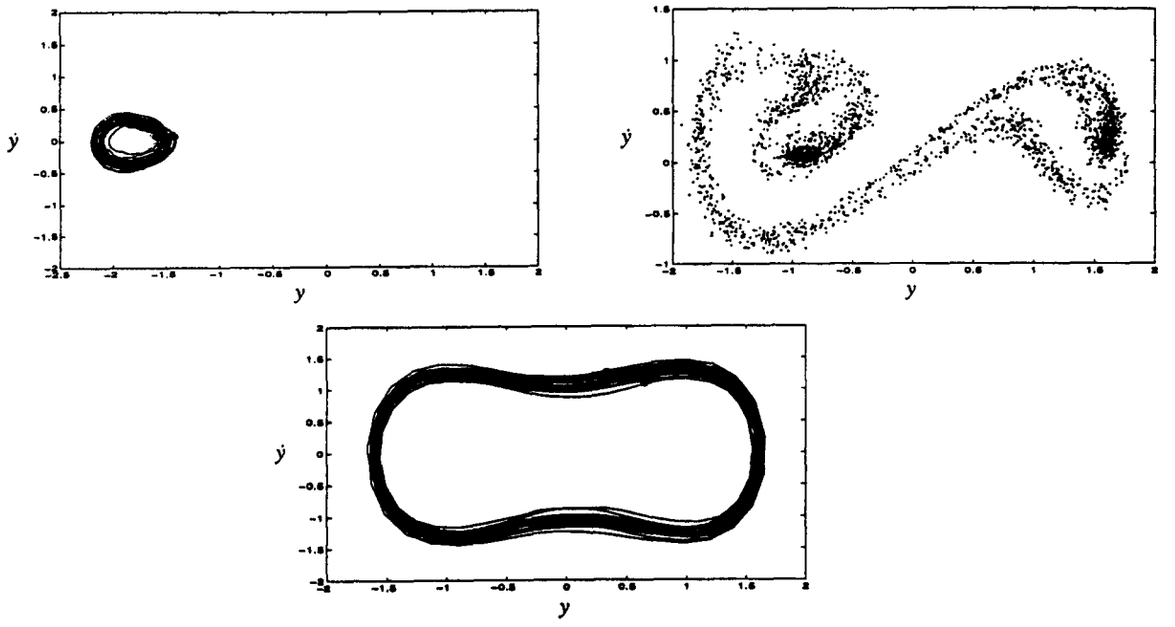

FIG. 15. Trajectories/Poincaré Maps for Eq. (1) over Range of Duffing Stiffness, d; For Chaotic Regime, Only Poincaré Map Is Shown ($\sigma_{ww} = 0.1$)

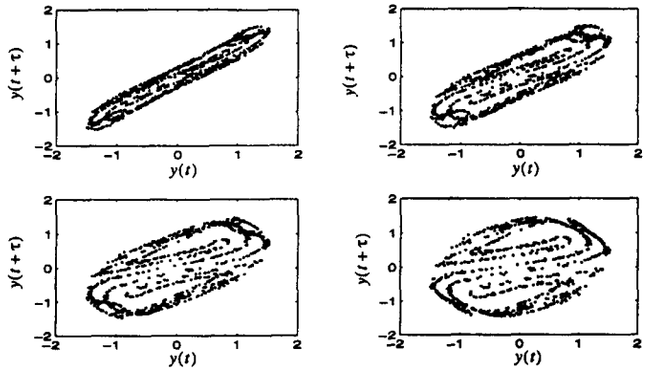

FIG. 16. Chaotic Attractor Observed in Fig. 7(a) when Observed Using Only Process Displacement in Two-Dimensional Reconstructed State-Space with Time Delays

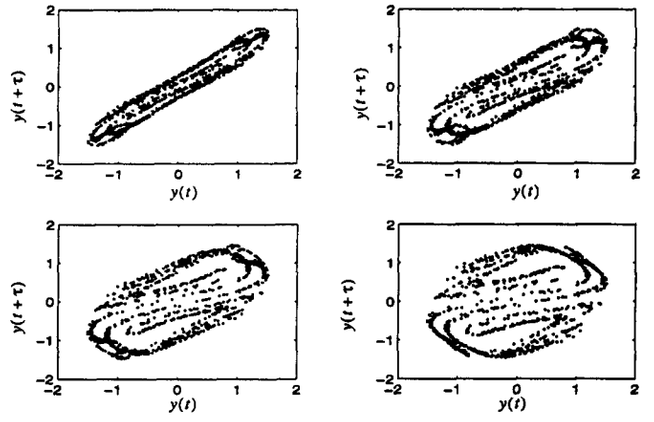

FIG. 17. Chaotic Attractor in Time-Delayed State Space where Gaussian White Noise of Standard Deviation 0.01 Has Been Added to Deterministic Excitation of System

due to the physical model or limitations in the measurement of experimental data, it has been shown (Takens 1981) that given a single process, $y(t_i)$, an m-dimensional phase vector may be constructed as

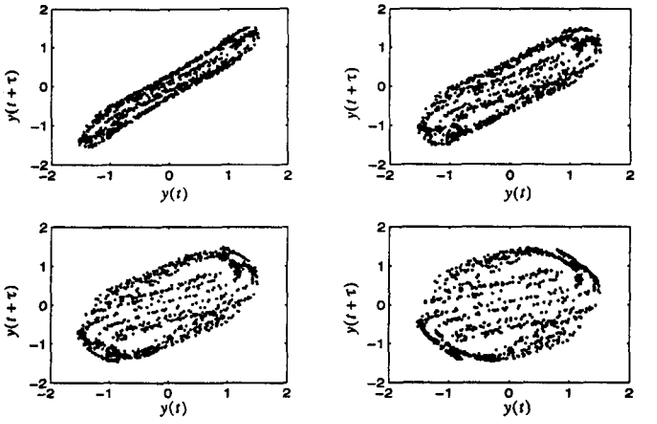

FIG. 18. Chaotic Attractor in Time-Delayed State Space where Gaussian White Noise of Standard Deviation 0.1 Has Been Added to Deterministic Excitation of System

$$Y(t_i) = \{y(t_i), y(t_i + \tau), \ldots, y[t_i + (m - 1)\tau]\} \qquad (11)$$

where τ = time delay. Some papers (e.g., Froehling et al. 1981; Liebert and Schuster 1989; Gershenfeld 1992; Poveda-Jaramillo and Puente 1993) have discussed systematic approaches for choosing a proper time delay and the merits thereof. A trial-and-error approach was taken according to the suggestions of Gershenfeld that in practical situations the delay should not be so small as to overly localize the analysis, nor too large that global effects cloud the desired results, but that over an intermediate range of time delay, the analysis is relatively invariant to the particular delay chosen. Favorable results have been noted using this approach as seen in Fig. 16, where the attractor in the previous case has been redrawn using two-dimensional time delay coordinates [see Fig. 7(a)]. Instead of using both the displacement and velocity of the process to produce this attractor, the displacement and its value after time delays, $\tau = T/8$, $T/4$, $3T/8$, $T/2$, where T is the natural period of the excitation. For very short time delays, the attractor is seen to be compressed around the diagonal of the space, however, for larger delays, the shape may be more clearly recognized as a transformed version of its representation in the original state space.

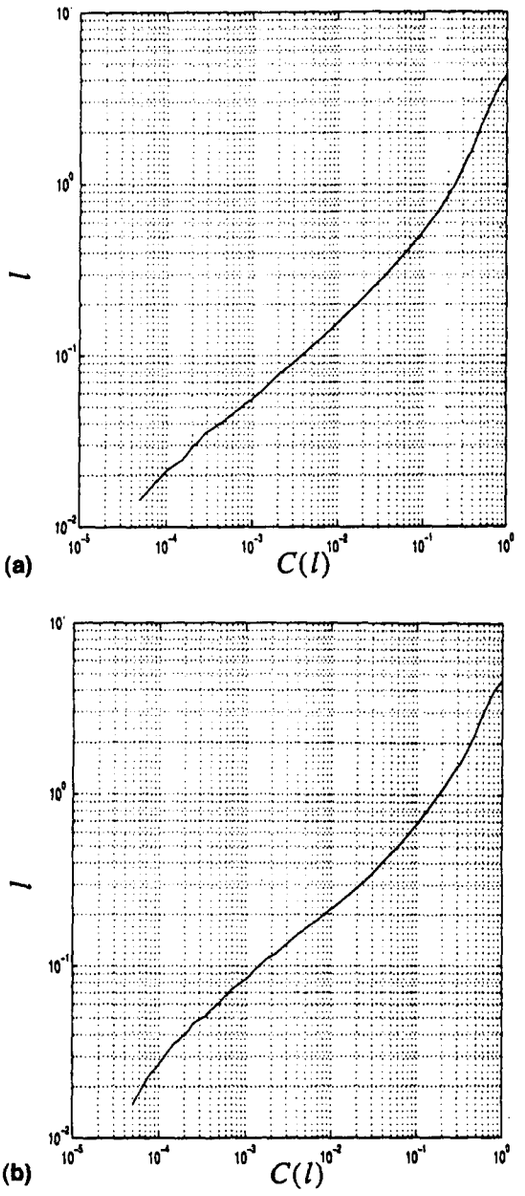

FIG. 19. Correlation Scaling Curves for Chaotic System: (a) in Four-Dimensional Reconstructed Phase Space, $\nu = 2.22$; (b) in Five-Dimensional Reconstructed Phase Space, $\nu = 2.50$ ($\tau = 7/8$)

Figs. 17 and 18 show that when Gaussian white noise is added to the input to the system, even at standard deviation comparable to that of the deterministic excitation, the attractor is still discernible from the data using the time-delay approach. It is still possible to observe underlying deterministic behavior in these types of cases using this approach.

Correlation Dimension of Attractor

The dimension of an attractor can yield much information concerning whether the motion of a system settles to a single point, is periodic, or chaotic. In addition, the dimension can yield information concerning whether or not a process is stochastic or possesses an underlying deterministic character. Many authors (e.g., Ben-Mizrachi et al. 1984; Casdagli 1989; Gershenfeld 1991; Poveda-Jaramillo and Puente 1993) have opted to use the correlation dimension, ν, where at a reference point, y_i

$$C_i(l) \equiv \lim_{N\to\infty} \frac{1}{N} \sum_{j=1, j\neq i}^{N} \theta(l - |y_i - y_j|) \tag{12}$$

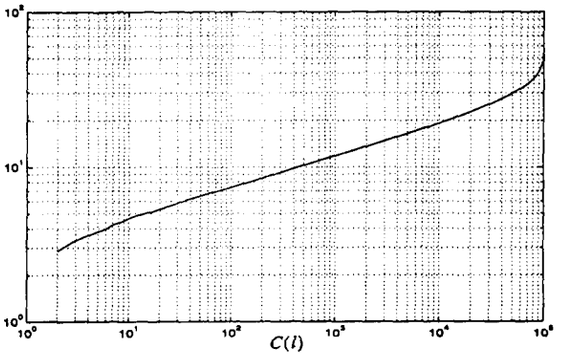

FIG. 20. Correlation Scaling Curve for Gaussian White Noise from which Five-Dimensional Phase Space Has Been Reconstructed, $\nu = 4.92$ ($\tau = 7/8$)

where N = total number of points in the time series; $\theta(x)$ = Heaviside step function; and the correlation scales as

$$C_i(l) \sim l^{\nu} \tag{13}$$

rather than the actual fractal dimension as an indicator of the system nature. The choice of the correlation dimension, rather than the fractal, is made due to the inefficiences in 'box-counting' methods for determining the former, as well as the tangible geometric pair-correlation, which is quantified by the latter. Although the two are, in general, not equal, it will be shown in the following discussion that the correlation dimension helps to make an adequate distinction between types of behavior in both deterministically and stochastically driven systems.

The correlation dimension, ν, may be determined by plotting, log $C_i(l)$ versus log l for one or more reference points in an attractor, and finding the slope. (The curve should be linear over a range of l characteristic of the attractor. This range may be determined by taking a numerical derivative. It is important to note that we are not talking about the slope of the curve across the entire range of l.) If the system state space has been properly reconstructed in d dimensions, then ν will properly characterize the dynamics of the system (i.e., $\nu = 0$ for a point, 1 for a line, 2 for a plane, etc., and has noninteger values for strange attractors). For a deterministic system, if we continue to increase the dimension, d, of the reconstructed state space using the techniques described in the preceding section, ultimately, ν will remain at a constant value no matter how large d becomes. Fig. 19 verifies this assertion. In this figure, once again, the deterministic chaotic example from the previous sections is utilized to illustrate that when the system state-space is reconstructed in four and five dimensions, respectively, the slope of the log-log plot remains at a lower value, $\nu \sim 2.21-2.50$. In this and all subsequent figures, the correlations shown will represent the average correlations over ten reference points. For a purely stochastic noise, the correlation will scale as

$$C_i(l) \sim l^{d} \tag{14}$$

Such a process is termed 'space filling.' This is illustated in Fig. 20 where a realization of Gaussian white noise has been used to reconstruct a five-dimensional state space and the slope of the log-log plot of correlation versus distance is 4.92. We cannot only tell different regimes of deterministic motion apart, but if the noise in our system is of a smaller length scale than that characterized by its deterministic component, we should be able to distinguish the presence of both in terms of a changing slope. That is, on a log-log plot, we should see a slope of ν until we reach length scales which are characteristic of the noise level in the system, where the slope should have a value of d (Ben-Mizrachi et al. 1984). Fig. 21 illustrates that

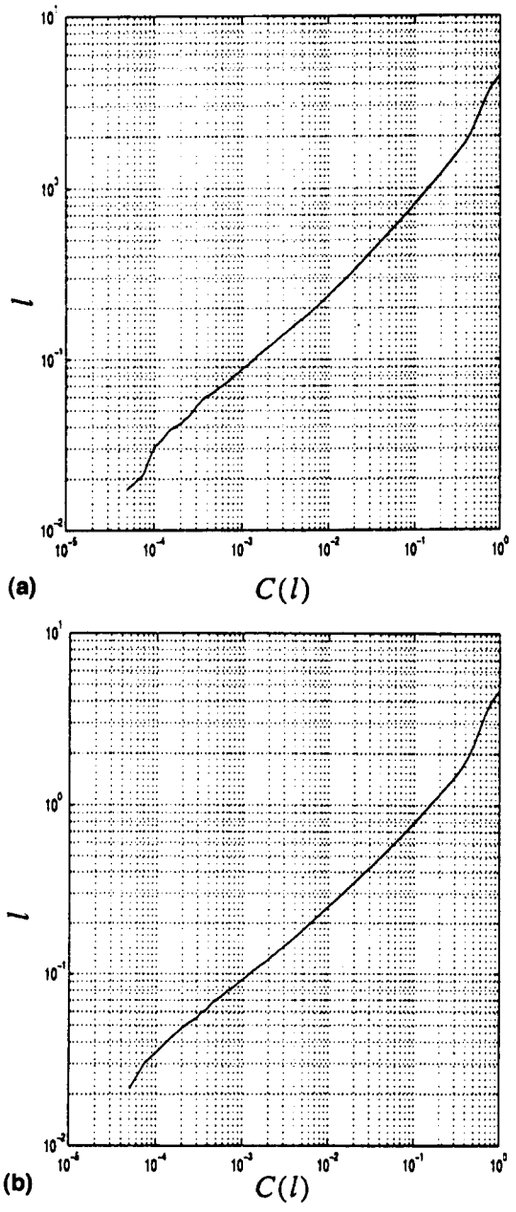

FIG. 21. Correlation Scaling Curve for Chaotic Attractor Using Five-Dimensional Reconstructed Phase Space: (a) Gaussian White Noise with Standard Deviation 0.01 Added, $\nu = 2.25$. ($\tau = 7$ 8)

for the case of the chaotic attractor of previous examples with different levels of Gaussian white noise added to the deterministic excitation of the system, the underlying deterministic nature of the system is detectable via the correlation dimension which remains around 2.30 for a five-dimensional embedding space. While the slope transition to a dimension characteristic of the noise is not discernible in this figure, it is hoped that when more extensive data sets are used, and the scaling curves are averaged over many more reference points, such a transition will be visible. This is a topic of future study.

The algorithm used in this study for calculating ν is based on that proposed by Gershenfeld (1991). First, a time series of a single state is used to reconstruct a higher dimensional state space using time-delay techniques. Next, one or more reference points are chosen at random and their distances (using a Euclidean norm) to all of the other points in the series is calculated. These distances are sorted in ascending order to yield l as a function of $C_i(l)$. The slope of this is ν^{-1}, the inverse of the correlation dimension. An average of the correlation values for each l at all of the reference points can yield a better approximation to the dimension.

One application of this technique could involve the analysis of random data to characterize the behavior of a practical nonlinear system by providing insight into the proper number of degrees of freedom necessary to model its governing equations, rather than immediately approximating it with a model whose physical basis may be questionable (Poveda-Jaramillo and Puente 1993).

CONCLUSIONS

The results presented in this paper indicate that several available techniques may be useful in analyses of physical systems modeled by nonlinear differential equations which are forced by both random and deterministic excitation. While the use of the variation of the PDF of the system response with time and averaged Poincaré mapping have been observed in the context of this study to be unreliable, as the random component of excitation becomes more important and perturbs the solution into different basins of attraction, many other techniques have proven satisfactory for the extraction of underlying determinism in the response. The most effective among the tools described are hypervolume analysis, attractor characterization using time-delay techniques, and correlation dimension analysis, all of which have been shown to indicate the presence of a deterministic structure in response motion, even when the strength of the random component of excitation becomes of an order comparable to the harmonic component. This study has been presented to demonstrate some of these techniques, their strengths, and their limitations. Clearly, more investigation is required in terms of developing a more thorough understanding, and a more systematic approach to applying them to physical systems. For example, correlation dimension analysis could be used to supplement hypervolume analysis when it is suspected that more than one regime of motion is exhibited by a system. In such a case, while the hypervolume only captures the attractor which occupies the largest hypervolume in phase space, the correlation dimension might take on different values at length scales, corresponding to the different regimes of motion. A Melnikov function-based approach (e.g., Frey and Simiu 1993) may also give insight into the transitions between regimes which are introduced by noise. These topic, however, are beyond the scope of the present work.

ACKNOWLEDGMENTS

This study was supported in part by ONR Grant No. 00014-93-1-0761. During the course of this study, the first writer was supported in part by a GAANNP fellowship.

APPENDIX. REFERENCES

Ben-Mizrachi, A., Procaccia, I., and Grassberger, P. (1984). "Characterization of experimental (noisy) strange attractors." *Physical Rev. A*, Am. Phys. Soc., 29(2), 975–977.

Casdagli, M. (1989). "Nonlinear prediction of chaotic time series." *Physica D*, Elsevier, D35, 335–356.

Ding, M., Ott, E., and Grebogi, C. (1994). "Controlling chaos in a temporally irregular environment." *Physica D*, Elsevier, 74, 386–394.

Frey, M., and Simiu, E. (1993). "Noise-induced chaos and phase space flux." *Physica D*, Elsevier, 63, 321–340.

Froehling, H., Crutchfield, J. P., Farmer, D., Packard, N. H., and Shaw, R. (1981). "On determining the dimension of chaotic flows." *Physica D*, Elsevier, 3D, 605–617.

Gershenfeld, N. A. (1992). "Dimension measurement on high-dimensional systems." *Physica D*, Elsevier, D55, 135–154.

Grebogi, C., Ott, E., and Yorke, J. A. (1987). "Chaos, strange attractors, and fractal basin boundaries in nonlinear dynamics." *Science*, 238, 632–637.

Jeffreys, E. R. (1988). "Nonlinear marine structures with random excitation." *J. Offshore Mech. & Arctic Engrg.*, ASME, 110, 246–253.
Kapitaniak, T. (1988). *Chaos in systems with noise*. World Scientific Publishing Co., Ltd., Teaneck, N.J.
Liebert, W., and Schuster, H. G. (1989). "Proper choice of the time delay for the analysis of chaotic time series." *Physics Lett.* A, Elsevier, 142(2, 3), 107–111.
MATLAB 4.2c User's Guide. (1992). The MathWorks, Inc.
Poveda-Jaramillo, G., and Puente, C. E. (1993). "Strange attractors in atmospheric boundary layer turbulence." *Boundary Layer Meteorology*, Kluwer Academic Publishers, 64, 175–197.
Sekar, P., and Narayanan, S. (1994). "Periodic and chaotic motions of a square prism in cross-flow." *J. of Sound and Vibration*, 170(1), 1–24.
SIMULINK User's Guide. (1992). The MathWorks, Inc.
Takens, F. (1981). *Springer lecture notes in mathematics*, D. A. Rand and L. S. Young, eds., Vol. 898, Springer, Berlin, 366–381.
Thompson, J. M. T., and Stewart, H. B. (1986). *Nonlinear dynamics and chaos: geometrical methods for scientists and engineers*. John Wiley & Sons, Inc., New York, N.Y.
Vaneck, T. (1994). "The hyper-volume method: finding boundaries between regular and chaotic phenomena in the forced Duffing oscillator." *J. of Sound and Vibration*, Academic Press, Inc., 175(4), 570–576.